Trajectory reversal approach for electron backscattering from solid surfaces

Wolfgang S. M. Werner*
Institut für Allgemeine Physik, Vienna University of Technology, Wiedner Hauptstraße 8-10, A 1040 Vienna, Austria
(Received 2 September 2004; published 15 March 2005)

The backscattering of medium energy electrons from solid surfaces is investigated by analysis of a linearized Boltzmann-type kinetic equation. A closed expression is derived for the Green's function in an infinite medium valid for a spherically symmetric potential describing the interaction with the ionic subsystem. The solution is expressed in terms of fluctuations of the energy loss and scattering angles and the collision statistics associated with them. Since the fluctuation part is independent of the boundary conditions of the considered problem, solution of the backscattering problem requires an appropriate treatment of the collision statistics. In this context, the exact solution for the Oswald–Kasper–Gaukler model is derived and its limitations are analyzed. An exact approach is presented and implemented in an efficient Monte Carlo scheme based on the trajectory reversal technique. The resulting procedure is faster than the conventional Monte Carlo algorithm by several orders of magnitude. Results for the angular distribution are compared with conventional Monte Carlo calculations and perfectly agree with the latter within their statistical uncertainty. A second approximate algorithm is also given. The approximation involved in this second procedure turns out to be very reasonable: deviations from direct Monte Carlo calculations remain below ~5% for energies exceeding 200 eV. The integral elastic-backscattering coefficient for normal incidence for a large number of materials in the energy range 50 eV–10 keV is found to approximately exhibit a universal dependence on the ratio of the inelastic and the transport mean free paths, the so-called scattering parameter.

DOI: 10.1103/PhysRevB.71.115415 PACS number(s): 68.49.Jk, 79.20.−m, 79.60.−i

I. INTRODUCTION

When a medium-energy (50 eV–10 keV) electron hits a solid surface, it strongly interacts with the ionic and electronic subsystems. The long-range part of the screened Coulomb potential of the ionic cores mainly affects the details of the small-angle part of the elastic-scattering cross section that are less important for the particle transfer. Therefore, when coherent scattering is insignificant, for example in polycrystalline or amorphous solids, the elastic cross section can be established *ab initio* on the basis of appropriately chosen potentials for *free* atoms.[1–6] Since the probability for (multiple) scattering increases monotonically with the path length traveled inside the solid, the probability for backscattering without energy loss depends not only on the elastic scattering cross section, but also on the value of the electron inelastic mean free path (IMFP). Since the former quantity can be calculated *ab initio*, the IMFP can be calibrated by measurements of the intensity of the peak of elastically backscattered electrons.

The potential of backscattering experiments for measurement of the IMFP was first recognized by Schilling and Webb.[7] Later, the importance of this technique [commonly referred to as Elastic Peak Electron Spectroscopy (EPES)] for nano-scale calibration by means of electron beam attenuation was realized by other authors and the technique was further investigated and developed.[1,2,8–11] It turns out that the elastic reflection coefficient depends approximately linearly on the IMFP[11] and the relative error in the IMFP is comparable to the relative error in the experimental reflection coefficient. To avoid absolute calibration of the experimental apparatus, which is a difficult task, the reflection coefficient is usually measured together with that for a reference material for which the IMFP is assumed to be known. In this way, the experimental error can be kept below 5% without much effort and the experimental contribution to the final uncertainty in the IMFP compares favorably with other experimental techniques to calibrate the IMFP, such as the overlayer method.[3,12–14]

On the theoretical side, an accurate model relating the experimental reflection coefficient to the IMFP is needed, as well as reliable data for the elastic scattering cross section which is needed as the only input parameter of such a model. In the present paper the focus will be on the model for elastic backscattering in noncrystalline solids assuming reliable data for the elastic cross section to be available.

The Monte Carlo (MC) technique is a convenient method to study transport phenomena within the framework of a Boltzmann-type kinetic equation where diffraction effects can be disregarded.[15] The MC technique is simple to implement and completely flexible with respect to the input parameters and, most importantly, with respect to the boundary conditions that can be arbitrarily complex. A disadvantage of this technique is that the influence of the input parameters on the outcome of a simulation is not physically evident and, most importantly, accumulation of the required statistical accuracy requires considerable computational effort. This is particularly problematic if the solid angle of the detector in the simulation is small, since then a large fraction of the simulated trajectories are generated in vain when they leave the solid in a direction not matching the analyzer acceptance angle. In the case of emission problems, this difficulty may be overcome by invoking the symmetry properties of the kinetic equation, the so-called reciprocity relationships for linear transfer.[16] One of these relationships can be interpreted to state that instead of simulating the electron from its point of emission inside the solid, and following the particle's path

until it eventually escapes from the surface in a direction not necessarily matching the analyzer acceptance angle, the trajectory can be generated in reverse, starting in the analyzer from where its history is traced back in the solid. By means of this trajectory reversal technique,[17–19] the angular distribution of Auger- or photoelectrons can be rapidly calculated for an arbitrarily small acceptance angle leading to an enhancement in computational efficiency of typically several orders of magnitude. Unfortunately, it is not straightforward to apply this procedure to reflection problems since the angular divergence in the electron source is usually even smaller than the detector acceptance angle.

Exact analytic solutions of the transport equation are very complex[20,21] and one is usually forced to make appropriate approximations. Several approximate analytical models for elastic backscattering have been published in the past.[22–28] Recently,[4] these models were critically evaluated and a comparison with MC calculations showed that the model by Oswald, Kasper, and Gaukler (OKG) (Refs. 2 and 26) gives the best agreement with the MC results. It was therefore recommended that the OKG model be used for determination of the IMFP by means of EPES. The OKG model is based on the assumption that only one of the elastic processes taking place in electron backscattering gives rise to a large deflection angle. OKG were able to find an analytic solution of their model by making the additional assumption that the loci of elastic collisions are equidistant, the length between them being equal to the total mean free path. Although this simple model works surprisingly well, significant deviations between the OKG and the MC approach have been observed that may exceed 30% in certain cases[4] and can be attributed to a deficiency in the treatment of multiple scattering in OKG's approach.

Recently, an alternative numerical approach based on the invariant embedding method was proposed[29] and was later successfully applied to elastic electron reflection.[30] This procedure is similar to the MC method in that it gives the exact solution within the numerical accuracy of the implementation. However, convergence is attained much faster than with the MC technique. The accuracy attainable in a practical calculation is much higher than with the MC technique and therefore it represents an atractive alternative to MC simulations, at least for cases with simple boundary conditions.

Another important aspect of the electron-backscattering process is the occurrence of surface excitations as the electron passes the solid-vacuum boundary on its way into and out of the solid,[29,31–33] leading to additional energy losses that must be accounted for in order to extract the proper inelastic mean free path for volume scattering from elastic-peak data. The surface-excitation probability depends on the distance from the surface in- and outside the solid, and therefore the electron-solid interaction parameters depend on the depth. Among the methods discussed above, the only one that can cope with such a situation is the MC technique which suffers from the inherent drawback of long computation times for practical calculations.

In the present work this problem is resolved by studying the kinetic equation and bringing it into a general form convenient for the application to electron-backscattering problems. In this way, the OKG model is solved exactly. Furthermore, an exact solution is given and implemented in a fast algorithm based on the trajectory-reversal principle. A second algorithm that involves an approximation is also derived. The accuracy of the approximation turns out to be reasonable: for energies exceeding 200 eV, the differential backscattering coefficient typically differs by less than 5% from results of direct MC calculations, while it is much faster. Therefore the proposed algorithms may be useful for the determination of the IMFP by means of EPES. Finally, the integral elastic-backscattering coefficient was calculated for normal incidence for a large number of materials in the energy range 50 eV–10 keV and was found to depend approximately universally on the ratio of the inelastic and the transport mean free paths, the so-called scattering parameter.

II. THEORY

A. Formal solution of the kinetic equation

Since the transport equation is linear, the solution satisfying the boundary conditions and source function for a specific problem can be found by superposition once the Green's function for the problem is known. In the present context, the Green's function is often referred to as the (generalized) loss function $G(s,T,\mu)$ that describes the distribution of energy losses T and net deflection angles $\theta=\arccos\mu$ after traveling a path length $s=|x-x'|$ in the solid. The Green's function will be derived for an infinite medium subject to the initial condition $G(s=0,T,\mu)=\delta(T)\delta(\mu)/4\pi$. Here and below the dependence on the azimuth will be suppressed since it is assumed that the scattering potential is radially symmetric, giving rise to a cylindrical symmetry of scattering. Keeping these assumptions in mind, standard arguments[34] can be used to write the kinetic equation for the generalized loss function in the form:

$$\frac{\partial G}{\partial s} = -\frac{1}{\lambda}\int_{-\infty}^{+\infty}\int_{4\pi}\{G(s,T,\mu) - G(s,T_1,\mu_1)\}w(T_2,\mu_2)d\mathbf{\Omega}_2 dT_2. \quad (1)$$

The energy loss and angular variables before (T_1,μ_1), during (T_2,μ_2) and after (T,μ) the collision are related via

$$T_2 = T - T_1,$$

$$\mu_2 = \mu_1\mu + \nu_1\nu\cos(\phi-\phi_1). \quad (2)$$

The symbols μ,ν are a shorthand notation for the cosine and sine functions of the polar direction respectively, ϕ_1 and ϕ are the azimuths, and $d\mathbf{\Omega}_2=d\mu_2 d\phi_2$. The quantity $w(T,\mu)=\lambda W(T,\mu)$ is the normalized inverse differential mean free path for scattering (i.e., the distribution of scattering angles and energy losses in individual collisions) and λ is the total mean free path

$$\frac{1}{\lambda} = \int_{-\infty}^{+\infty}\int_{4\pi} W(T,\mu)d\mathbf{\Omega}dT. \quad (3)$$

Note that at this stage, no distinction has been made between different types of scattering such as elastic and inelastic scat-

tering. In consequence the interaction parameters referred to in the above, such as the differential inverse mean free path $w(T,\mu)$ and the total mean free path λ pertain to collisions of any kind.

Equation (1) is readily solved in Fourier-Legendre (FL) space.[35] The expansion coefficients $\widetilde{G}_l(p)$ are found by multiplying with $e^{-ipT}P_l(\mu_2)$, where $P_l(\mu)$ are the Legendre polynomials, and integrating over T and $\mathbf{\Omega}_2$. This yields:

$$\frac{\partial \widetilde{G}_l(p)}{\partial s} = -\frac{\widetilde{G}_l(p)}{\lambda}\{1-\widetilde{w}_l(p)\}, \tag{4}$$

where the quantities $\widetilde{w}_l(p)$ represent the FL-expansion coefficients of the normalized differential mean free path. The solution satisfying the initial condition in FL-space $\widetilde{G}_l(p,s=0)=1$ reads:

$$\widetilde{G}_l(p) = e^{-s/\lambda\{1-\widetilde{w}_l(p)\}}. \tag{5}$$

Going back to real space results in

$$G(s,T,\mu) = \sum_{l=0}^{\infty} \frac{2l+1}{8\pi^2} P_l(\mu) \int_{-\infty}^{+\infty} e^{ipT-s/\lambda\{1-\widetilde{w}_l(p)\}} dp. \tag{6}$$

To bring this expression into a more tractable form, the exponent is expanded with respect to its last term

$$G(s,T,\mu) = \sum_{N=0}^{\infty} \frac{e^{-s/\lambda}}{N!}\left(\frac{s}{\lambda}\right)^N \sum_{l=0}^{\infty} \frac{2l+1}{8\pi^2} P_l(\mu) \int_{-\infty}^{+\infty} e^{ipT} \widetilde{w}_l^N(p) dp, \tag{7}$$

where N denotes the number of collisions of any type. The second sum represents the $(N-1)$-fold self-convolution of the differential mean free path, denoted by $\Gamma_N(T,\mu)$. Introducing the collision number distribution $W_N(s)$, that describes the N-fold scattering probability as a function of the traveled path length,

$$W_N(s) = \frac{e^{-s/\lambda}}{N!}\left(\frac{s}{\lambda}\right)^N, \tag{8}$$

one can write the loss function in the form

$$G(s,T,\mu) = \sum_{N=0}^{\infty} W_N(s)\Gamma_N(T,\mu). \tag{9}$$

Physically, Eq. (9) states that the distribution of energy losses and deflection angles after a certain path length can be expressed in terms of the fluctuations in the energy loss and deflection angles after N losses, described by the self-convolution of the mean free path $\Gamma_N(T,\mu)$, and weighted with the collision statistics, i.e., the probability $W_N(s)$ that N collisions occur for the considered path length.

If the interaction is characterized by large energy transfers accompanied by small momentum transfers and vice versa, the energy loss and scattering angles in Eq. (9) can be decoupled, by making a distinction between *elastic* and *inelastic* collisions. For medium energy electrons in solids, this is always justified since the recoil energy loss in an elastic collision (when elastic scattering is defined as an interaction with the ionic subsystem of the solid), is orders of magnitude smaller than any energy loss suffered during interaction with the electronic subsystem. Then the angular and energy parts of the interaction can be separated by writing the normalized differential mean free path in the following form:

$$w(T,\mu) = \frac{\lambda}{\lambda_i} w_i(T)\frac{\delta(\mu)}{4\pi} + \frac{\lambda}{\lambda_e} w_e(\mu)\delta(T). \tag{10}$$

Here the subscripts "*i*" and "*e*" indicate inelastic and elastic scattering, λ_e and λ_i denote the elastic and inelastic mean free path, respectively, $w_i(T)$ is the usual normalized differential inverse inelastic mean free path, and $w_e(\mu)$ is the normalized elastic scattering cross section.

Inserting the above expression into Eq. (9) and using the well known identity

$$W_n(s_1+s_2) = \sum_{k=0}^{n} W_k(s_1)W_{n-k}(s_2), \tag{11}$$

the loss function can be written as

$$G(s,T,\mu) = \sum_{n_i=0}^{\infty} W_{n_i}^i(s)\Gamma_{n_i}^i(T) \sum_{n_e=0}^{\infty} W_{n_e}^e(s)\Gamma_{n_e}^e(\mu), \tag{12}$$

where (n_i) and (n_e) denote the number of inelastic and elastic collisions after $N(=n_i+n_e)$ arbitrary collisions, respectively. Here and below, the superscripts "*i*" and "*e*" are used to make the distinction between inelastic and elastic scattering, respectively. The functions $W_{n_i}^i(s)$ and $W_{n_e}^e(s)$ correspond to the stochastic processes for inelastic and elastic scattering that are given in the quasielastic regime by Eq. (8) by replacing the total mean free path λ by λ_i and λ_e, respectively. Likewise, the functions Γ_{n_i} and Γ_{n_e} now represent the self-convolutions of the inelastic and elastic terms of the total differential mean free path. The second factor represents the path length distribution in an infinite medium, $Q(s,\mu)$,[36]

$$Q(s,\mu) = \sum_{n_e=0}^{\infty} W_{n_e}^e(s)\Gamma_{n_e}^e(\mu) \tag{13}$$

and the formal solution of the kinetic equation reads

$$G(s,T,\mu) = \sum_{n_i=0}^{\infty} W_{n_i}^i(s)\Gamma_{n_i}^i(T)Q(s,\mu). \tag{14}$$

The form Eq. (12) of the solution of the transport equation makes it clear that the influence of the boundary conditions is reflected only through the collision statistics: the energetic fluctuations depend on the respective differential mean free paths and collision number only. Since the collision statistics depend on the traveled path length only, it suffices to find the path length distribution. If the path length distribution is known for a particular problem, the above expression allows us to find the specific solution by superposition. However, deriving an expression for the path length distribution for a particular set of boundary conditions in general represents a formidable task and often one is forced to resort to numerical calculations or simplifying assumptions, as discussed in the next sections.

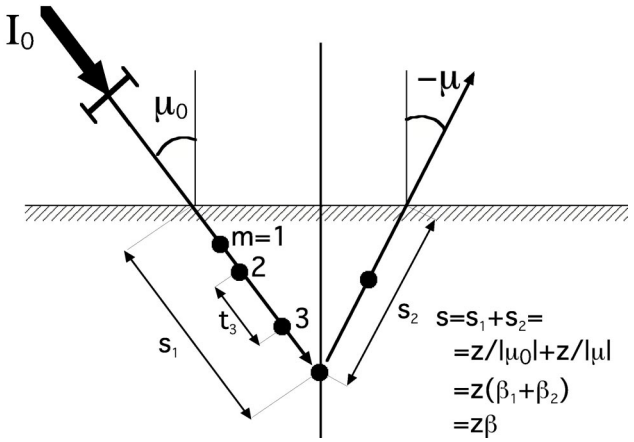

FIG. 1. Schematic illustration of the single large-angle collision model for elastic backscattering of Oswald, Kasper, and Gaukler (Ref. 26).

Introducing the partial intensities C_{n_i} as the number of electrons that arrive in the detector after experiencing a certain number of inelastic collisions for the specific boundary conditions and taking into account the linearity of the kinetic equation

$$C_{n_i} = \int_0^\infty W^i_{n_i}(s) Q(s) ds, \tag{15}$$

the observed spectrum can be written in the convenient form

$$Y(E) = \sum_{n_i=0}^{\infty} C_{n_i} \Gamma^i_{n_i}(T) \otimes f_0(E+T), \tag{16}$$

where $f_0(E)$ is the energy distribution at the source and the symbol $\otimes$ denotes a convolution over the energy variable.

B. The Oswald–Kasper–Gaukler (OKG) model

Oswald, Kasper, and Gaukler [2,26] observed that the major contribution to the elastic backscattering coefficient comes from trajectories that only participate in a few ($n_e \sim 1-3$) elastic collisions, their relative intensity rapidly decreasing with the order of elastic scattering. According to Eq. (13) the net deflection in a backscattering process is then mainly determined by the first order term, the elastic scattering cross section, since for $n_e=0$ no backscattering occurs. This implies that all elastic processes, except one, lead to a negligible deflection. This single large–angle scattering model due to OKG is schematically illustrated in Fig. 1. In their approach to evaluate this model, OKG were forced to make an additional approximation in order to arrive at a closed expression for the partial backscattering coefficient η_{n_e} after n_e-fold elastic scattering. To integrate Eq. (28) in Ref. 26, it was assumed that the path length between any two successive elastic events is equal to the total mean free path $\lambda = 1/(\lambda_e^{-1}+\lambda_i^{-1})$ (p. 75 in Ref. 2). Although Oswald's derivation is distinctly clear,[2] it is rather lengthy and the effect of the additional assumption made is not obvious. Since it has been recommended to use this approach for quantitative application in EPES,[4] it seems worthwhile to investigate this model in more detail.

Within the formalism outlined in the present work, there is no need to make any additional assumptions and the partial reflection coefficient is easily obtained in closed form. This is possible since for the OKG model, a fixed relationship exists between the depth of backscattering and the corresponding path length (see Fig. 1).

Any reflected trajectory in which n_e collisions occur is characterized by m elastic collisions on the way in, one collision at the depth z and n_e-m-1 collisions on the way out. Obviously, n_e different values of m are possible. From Eq. (13) it follows that the probability for reaching the depth z in the direction $\mathbf{\Omega}'$ after m-fold scattering is just $W^e_m[s_1(z)]\Gamma^e_m(\mathbf{\Omega}_0,\mathbf{\Omega}')$. Likewise, for an electron starting at the depth z in the direction $\mathbf{\Omega}''$, the probability to escape in the direction $\mathbf{\Omega}$ after n_e-1-m collisions is given by $W^e_{n_e-1-m}[s_2(z)]\Gamma^e_{n_e-1-m}(\mathbf{\Omega}'',\mathbf{\Omega})$. Here $s_1(z)$ and $s_2(z)$ are the path lengths traveled along the in- and outgoing part of the trajectory. Since the probability for a directional change $(\mathbf{\Omega}' \to \mathbf{\Omega}'')$ is just $\Gamma^e_1(\mathbf{\Omega}',\mathbf{\Omega}'')/\lambda_e$, the partial path length distribution Q_{n_e} for n_e-fold elastically scattered electrons is given by

$$\begin{aligned} Q_{n_e}(s(z),\mathbf{\Omega}_0,\mathbf{\Omega}) = \frac{1}{n_e}\sum_{m=0}^{n_e-1} & \Gamma^e_m(\mathbf{\Omega}_0,\mathbf{\Omega}')W^e_m[s_1(z)] \\ & \otimes \frac{\Gamma^e_1(\mathbf{\Omega}',\mathbf{\Omega}'')}{\lambda_e} \\ & \otimes \Gamma^e_{n_e-1-m}(\mathbf{\Omega}'',\mathbf{\Omega})W^e_{n_e-m-1}[s_2(z)]. \end{aligned} \tag{17}$$

Note that here and below $\mathbf{\Omega}_0=(\arccos\mu_0,\phi_0)$ and $\mathbf{\Omega}=(\arccos\mu,\phi)$ are used to indicate the incoming and outgoing direction of motion, while in the preceding section μ was used to indicate a directional *change* during a deflection. The convolutions in Eq. (17), denoted by the symbol $\otimes$ concern the polar and azimuthal angular variables integrated over the unit sphere.

At this stage, the two main implications of the OKG model assumptions come into play: (1) since only one collision is assumed to contribute significantly to the net deflection, all deflection angles along s_1 and s_2 are small and equal for any value of m. Then, the angular terms may be taken outside the sum and combined into a factor $\Gamma_{n_e}(\mathbf{\Omega}_0,\mathbf{\Omega})$; (2) The path length elongation along s_1 and s_2 due to the finite scattering angles is neglected, leading to a drastic simplification of the relationship between the traveled path length and the depth (see Fig. 1):

$$\begin{aligned} s_1(z) &\approx \beta_1 z, \\ s_2(z) &\approx \beta_2 z, \end{aligned} \tag{18}$$

where $\beta_1=1/|\mu_0|$, $\beta_2=1/|\mu|$, and $\beta=\beta_1+\beta_2$. Then, the partial elastic reflection coefficient $\eta_{n_e}=C_{n_e,n_i=0}(\mathbf{\Omega}_0,\mathbf{\Omega})$ is found by inserting the average path length distribution into Eq. (15) with $n_i=0$:

$$\eta_{n_e}(\mathbf{\Omega}_0,\mathbf{\Omega}) = \frac{1}{|\mu_0|}\frac{\Gamma^e_{n_e}(\mathbf{\Omega}_0,\mathbf{\Omega})}{\lambda_e} \times \int_0^\infty W^i_0(\beta z)\frac{1}{n_e}\sum_{m=0}^{n_e-1} W^e_m(\beta_1 z)W^e_{n_e-m-1}(\beta_2 z)dz, \tag{19}$$

where the factor $1/|\mu_0|$ accounts for flux conservation at the surface (see Fig. 1). Using the quasielastic expression for the stochastic process [Eq. (8)] and performing the elementary integration leads to the result

$$\eta_{n_e}(\mathbf{\Omega}_0,\mathbf{\Omega}) = \frac{|\mu|}{|\mu_0|+|\mu|}\frac{\Gamma^e_{n_e}(\mathbf{\Omega}_0,\mathbf{\Omega})}{n_e}\left(\frac{\lambda}{\lambda_e}\right)^{n_e}. \tag{20}$$

This is identical to expression (31) in Ref. 26. Thus it turns out that the additional approximation of equal step-lengths, made in Oswald's derivation, leads to the exact solution of the OKG model.

C. Trajectory reversal approach

In the OKG model an effective approximation of the function $s(z)$ gives rise to an analytic expression for the partial reflection coefficient that is reasonably accurate. If a higher accuracy is required, the function $s(z)$ must somehow be established numerically and inserted in Eq. (17). Note that the latter equation is exact. Since the explicit form of $s(z)$ is not of main interest, it is convenient to introduce the notation $\psi_m(z,\mathbf{\Omega}_0,\mathbf{\Omega}')$ and $\psi^*_{n_e-m-1}(z,\mathbf{\Omega},\mathbf{\Omega}'')$ for the exact depth distribution functions $W^e_m[s_1(z)]\Gamma^e_m$ and $W^e_{n_e-m-1}[s_2(z)]\Gamma^e_{n_e-m-1}$ in the following. The function $\psi_m(z,\mathbf{\Omega}_0,\mathbf{\Omega}')$ describes the probability for an electron incident on the surface in the direction $\mathbf{\Omega}_0$ to arrive at the depth z with the direction $\mathbf{\Omega}'$ after m elastic collisions. Conversely, $\psi^*_m(z,\mathbf{\Omega},\mathbf{\Omega}'')$ represents the probability distribution for an electron that starts at the depth z in the direction $\mathbf{\Omega}''$ to reach the surface with a direction $\mathbf{\Omega}$ after m collisions. For the following it is essential to note that by virtue of the reciprocity theorem for one-speed transport,[16] the in- and outgoing depth distributions are related by

$$\psi^*_m(z,\mathbf{\Omega}',\mathbf{\Omega}) = |\mu'|\psi_m(z,\mathbf{\Omega},\mathbf{\Omega}'), \tag{21}$$

where $\mu' = (\mathbf{\Omega}'\cdot\mathbf{n}_z)$ is the polar emission direction and $\mathbf{n}_z$ is the unit vector along the surface normal. Each trajectory can be divided into an in- and outgoing part separated by a scattering event at the depth z, characterized by the directions $\mathbf{\Omega}'$ and $\mathbf{\Omega}''$ before and after the collision. Note that this depth is not necessarily the largest depth reached by the particle, as in the OKG model. With the aid of the depth distributions, the formula for the partial path length distribution [Eq. (17)] can be rewritten as

$$Q_{n_e}(s(z),\mathbf{\Omega}_0,\mathbf{\Omega}) = \frac{1}{n_e}\sum_{m=0}^{n_e-1}\psi_m(z,\mathbf{\Omega}_0,\mathbf{\Omega}')\otimes\frac{\Gamma^e_1(\mathbf{\Omega}',\mathbf{\Omega}'')}{\lambda_e} \otimes \psi^*_{n_e-m-1}(z,\mathbf{\Omega},\mathbf{\Omega}''). \tag{22}$$

This equation is exact and ideally suited for calculation by means of a rapid MC algorithm based on the trajectory reversal technique. The resulting procedure (referred to as Algorithm I below) is *exactly* equivalent to the conventional MC procedure, but is faster by typically several orders of magnitude, in particular for small detector solid angles.

A simplifying assumption can be made at this stage which does not lead to a serious loss of accuracy and gives rise to an effective approximation (referred to as Algorithm II below). It consists of replacing the depth distribution $\psi_m(z,\mathbf{\Omega}_0,\mathbf{\Omega}')$ by its average over $\mathbf{\Omega}'$, denoted as $\psi_m(z,\mathbf{\Omega}_0)$, multiplied with the angular fluctuation factor $\Gamma^e_m(\mathbf{\Omega}_0,\mathbf{\Omega}')$,

$$\psi_m(z,\mathbf{\Omega}_0,\mathbf{\Omega}') \approx \psi_m(z,\mathbf{\Omega}_0)\Gamma^e_m(\mathbf{\Omega}_0,\mathbf{\Omega}'). \tag{23}$$

An equivalent expression holds for the function $\psi^*_m(z,\mathbf{\Omega},\mathbf{\Omega}'')$. Then, the expression for the partial path length distribution becomes

$$Q_{n_e}(s(z),\mathbf{\Omega}_0,\mathbf{\Omega}) = \frac{\Gamma^e_{n_e}(\mathbf{\Omega}_0,\mathbf{\Omega})}{n_e\lambda_e}\sum_{m=0}^{n_e-1}\psi_m(z,\mathbf{\Omega}_0)\psi^*_{n_e-1-m}(z,\mathbf{\Omega}), \tag{24}$$

which is exact for $n_e=1$ since in this case one always has $\mathbf{\Omega}_0=\mathbf{\Omega}'$ and $\mathbf{\Omega}''=\mathbf{\Omega}$. Furthermore, the neglect of the proper angular correlation in Eq. (23) is expected to be approximately justified also for higher order scattering since the elastic cross section is strongly peaked in the forward direction. Thus the approximation involved in Algorithm II accounts for the path length elongation along the trajectory due to finite scattering angles, but neglects the proper angular correlations along the trajectory. Since the OKG model neglects both the angular correlation as well as the path length elongation, Algorithm II is expected to be more accurate than the OKG model. Inserting the sum of the partial path length distributions into Eq. (15), the elastic reflection coefficient within Algorithm II is finally found as

$$\eta_e(\mathbf{\Omega}_0,\mathbf{\Omega}) = \sum_{n_e=1}^{\infty} B_{n_e}(\mathbf{\Omega}_0,\mathbf{\Omega})\Gamma^e_{n_e}(\mathbf{\Omega}_0,\mathbf{\Omega}), \tag{25}$$

where the coefficients $B_{n_e}(\mathbf{\Omega}_0,\mathbf{\Omega})$ are given by

$$\begin{aligned} B_{n_e}(\mathbf{\Omega}_0,\mathbf{\Omega}) &= \frac{1}{\lambda_e n_e}\int\sum_{m=0}^{n_e-1}\Psi_m(z,\mathbf{\Omega}_0)\Psi^*_{n_e-1-m}(z,\mathbf{\Omega})dz \\ &= \frac{1}{\lambda_e n_e}\int\sum_{m=0}^{n_e-1} W^i_0[s_1(z)]\psi_m(z,\mathbf{\Omega}_0)W^i_0 \\ &\quad\times[s_2(z)]\psi^*_{n_e-1-m}(z,\mathbf{\Omega})dz. \end{aligned} \tag{26}$$

Recalling that $W^i_0[s_1(z)]\cdot W^i_0[s_2(z)] = W^i_0[s(z)]$, it is seen that the latter expression is very similar to the OKG result Eq. (19). The essential difference is that Eq. (26) accounts for the path length elongation along the trajectory and is therefore expected to yield a better description of multiple scattering than the OKG model.

III. NUMERICAL IMPLEMENTATION

The OKG model as well as Algorithm I and II proposed in the present work were implemented and compared with con-

TABLE I. Parameters describing the elastic and inelastic interaction for medium energy electron transport in Be and Au. The elastic, inelastic, and transport mean free paths are denoted by λ_e, λ_i, and λ_{tr}, respectively, and are given in units of Å, while $\chi=\lambda_i/\lambda_{tr}$ is the scattering parameter in the quasielastic energy regime.

	Be				Al				Cu				Au			
E(eV)	λ_e	λ_i	λ_{tr}	χ	λ_e	λ_i	λ_{tr}	χ	λ_e	λ_i	λ_{tr}	χ	λ_e	λ_i	λ_{tr}	χ
100	2.9	5.5	9.9	0.56	3.3	5.3	7.9	0.67	4.1	4.1	7.0	0.59	2.0	5.6	10.4	0.54
150	3.9	6.7	17.9	0.37	4.0	6.4	11.9	0.54	4.2	4.7	7.4	0.63	2.5	6.1	18.1	0.34
300	6.8	10.1	53.1	0.19	6.1	9.8	27.0	0.36	5.2	6.8	10.6	0.64	3.8	8.3	18.6	0.45
500	10.6	14.5	124	0.12	8.5	14.0	53.1	0.26	6.6	9.5	16.7	0.57	5.4	11.3	16.7	0.68
1000	20.3	24.5	414	0.06	13.8	23.7	143	0.17	9.4	15.5	37.1	0.42	7.6	18.2	23.8	0.77
2000	39.5	42.7	1418	0.03	23.4	41.2	416	0.10	13.7	26.5	94.2	0.28	10.2	30.7	47.0	0.65
5000	95.9	91.5	7401	0.01	49.8	87.8	1888	0.05	23.6	55.5	367	0.15	15.5	63.4	146	0.43

ventional Monte Carlo calculations for electrons in the energy range 100–5000 eV backscattered from Be, Al, Cu, and Au surfaces. The angular distribution was calculated in the plane of incidence in 4° steps for an analyzer with a circular aperture described by a full polar opening angle of 4°. Calculations were performed for normal as well as oblique incidence (60° and 75°).

The input parameters are the same for the three models and comprise the electron inelastic mean free path calculated by the TPP-2M formula[37] and the elastic scattering cross section that was calculated using the computer code of Ref. 38 for a Thomas–Fermi–Dirac potential. The resulting inelastic (λ_i), elastic (λ_e) and transport mean free paths (λ_{tr}) as well as the scattering parameter $\chi=\lambda_i/\lambda_{tr}$ are shown for the investigated materials in Table I.

The algorithm for the conventional Monte Carlo simulations has been described in detail before,[5,11] it is merely noted here that 10^7 trajectories were required to accumulate reasonable statistics for Cu and Au, while for Be and Al, that have a significantly lower reflection coefficient in this energy range, 10^8 trajectories were simulated.

For the implementation of the OKG model, multiple self-convolutions of the elastic cross section need to be performed. In the present work, this was achieved by expanding the cross section in a series of Legendre polynomials. The n_e-fold convolution of the cross section is then given by the Legendre back-transform of the n_e-th power of the expansion coefficients.[4,9,35]

For the approximate model proposed in this work (Algorithm II), the coefficients B_{n_e} [Eq. (26)] need to be calculated in addition. In principle, this can be done by establishing the path length distribution using Eq. (24) and applying the formalism outlined in the theory section. However, it is more convenient to directly calculate the coefficients B_{n_e}. This can be achieved with a Monte Carlo technique by generating a set of trajectories in the usual way, keeping track of the traveled path length along the trajectory as well as the number of elastic processes m that has taken place. The trajectory is terminated when the contribution to B_m becomes insignificant, i.e. when the traveled path length exceeds the inelastic mean free path by a factor $5\times n_e$, or when it leaves the solid again. The solid is divided into thin slabs of thickness Δz. In each depth interval k penetrated by the particle, the contribution to the coefficient $\Psi_{m,k}$ is directly evaluated via

$$\Delta\Psi_{m,k}=\frac{1}{\mu_k}\exp(-s(z_k)/\lambda_i),$$

where the polar direction along the kth interval μ_k accounts for flux conservation and $s(z_k)$ is the total path length traveled when reaching the kth depth, respectively. In other words, instead of explicitly calculating the depth distributions, the product of the depth distribution and the inelastic collision statistics is directly evaluated by this algorithm

$$\Psi_{m,k}(\mathbf{\Omega})=W_0^i[s(z_k)]\psi_m(z_k,\mathbf{\Omega}). \tag{27}$$

In this way, one of the most difficult aspects of transport problems is circumvented: the conversion between depth and traveled path length. The outgoing depth distribution is calculated in exactly the same way, starting the trajectory in the detector and tracing it back into the solid. The starting directions for the outgoing probability $\Psi^*_{m,k}(\mathbf{\Omega})$ are uniformly sampled from directions around $\mathbf{\Omega}$ that lie within the detector solid angle $\Delta\Omega$. Afterwards this in-going depth distribution is converted into an outgoing one by invoking the reciprocity relationship Eq. (21). The histograms for the in- and outgoing probabilities are eventually combined to give the required coefficients

$$B_{n_e}(\mathbf{\Omega}_0,\mathbf{\Omega})=\frac{\Delta z\Delta\Omega}{\lambda_e n_e}\sum_{k=0}^{k_{\max}}\sum_{m=0}^{n_e-1}\Psi_{m,k}(\mathbf{\Omega}_0)|\mu|\Psi_{n_e-1-m,k}(\mathbf{\Omega})/N_{\text{traj}}^2, \tag{28}$$

where the number of trajectories N_{traj} and solid angle of detection $\Delta\Omega$ ensure proper normalization. The factor $|\mu|$ effects the trajectory reversal of the outgoing distribution. For all results in the present paper $N_{\text{traj}}=10^4$ trajectories were sufficient to achieve the required statistical accuracy of $<1\%$.

To obtain the elastic reflection coefficient by means of Algorithm I, the path length distribution Eq. (22) is inserted into Eq. (15). Thus, the matrix Ψ_{m,n_e} defined through

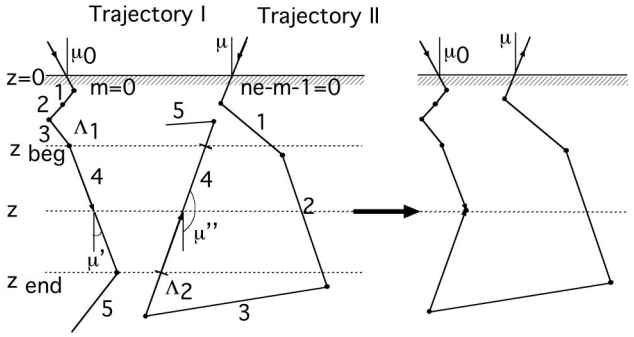

FIG. 2. Illustration of the evaluation of overlapping segments of a trajectory pair (see text).

$$\Psi_{m,n_e} = \int_0^\infty W_0^i[s(z)]\psi_m(z,\mathbf{\Omega}_0,\mathbf{\Omega}') \otimes \frac{\Gamma_1^e(\mathbf{\Omega}'\cdot\mathbf{\Omega}'')}{\lambda_e} \otimes \psi^*_{n_e-m-1}(z,\mathbf{\Omega},\mathbf{\Omega}'')dz \tag{29}$$

needs to be evaluated. The quintuple integration in Eq. (29) can also be carried out by means of an efficient trajectory reversal Monte Carlo procedure. This can be done by generating trajectory *pairs* in the usual way (see Fig. 2) and realizing that every step of trajectory I between the mth and $(m+1)$st collision gives a contribution to the depth distribution $\psi_m(z,\mathbf{\Omega}_0,\mathbf{\Omega}')$ at *any* depth $z_m \leqslant z \leqslant z_{m+1}$, while the same is true for trajectory II that contributes to the outgoing depth distribution $\psi^*_{n_e-m-1}(z,\mathbf{\Omega},\mathbf{\Omega}'')$ at *any* depth penetrated by the (n_e-m-1)th step. Combining trajectories at any depth reached by both of them is effected by multiplying with the probability $\Gamma_1^e(\mathbf{\Omega}'\cdot\mathbf{\Omega}'')/\lambda_e$ for a directional change from $\mathbf{\Omega}'$ to $\mathbf{\Omega}''$. For a given trajectory pair, all possible combined trajectories are found by determining the overlapping step segments for all steps taken by trajectory I. For the considered step shown in Fig. 2 this gives a contribution to $n_e=4$ for the in-going and $n_e-m-1=4$ for the outgoing part of the trajectory. Two additional contributions for the fourth step of the in-going trajectory come from $n_e-m-1=1$ and $n_e-m-1=2$ of the outgoing trajectory. Thus, each trajectory pair is ultimately combined into an infinite number (at least one for each overlapping depth) of reflected trajectories with different collision orders. For each overlapping trajectory pair segment, the total contribution to the elastic reflection coefficient can be calculated analytically. For any overlapping segment with scattering order (m,n_e), the contribution to the matrix Ψ_{m,n_e} is given by

$$\Delta\Psi_{m,n_e} = \frac{\Gamma_1^e(\mathbf{\Omega}'\cdot\mathbf{\Omega}'')}{\lambda_e|\mu'||\mu''|}\int_0^{\Delta z} W_0^i[s(z)]dz, \tag{30}$$

where $\Delta z=|z_{\text{beg}}-z_{\text{end}}|$ is the depth interval of the step of trajectory I and the factor $|\mu'||\mu''|$ accounts for flux conservation of the overlapping segment pair. The integral along each overlapping segment in Eq. (30) is easily evaluated analytically since the traveled path length for any depth joining the pair is given by a simple linear relationship:

TABLE II. Parameters α and β of Eq. (32) for different combinations of the polar directions μ' and μ'' of overlapping segments of a trajectory pair.

μ'	$\mu'\cdot\mu''$	α	β
$\geqslant 0$	$\geqslant 0$	0	$1/\lvert\mu'\rvert + 1/\lvert\mu''\rvert$
$\geqslant 0$	<0	$1/\lvert\mu''\rvert$	$1/\lvert\mu'\rvert$
<0	<0	$1/\lvert\mu'\rvert$	$1/\lvert\mu''\rvert$
<0	$\geqslant 0$	$1/\lvert\mu'\rvert + 1/\lvert\mu''\rvert$	0
μ''	$(\mu'')^2$	$1/\lvert\mu'\rvert$	0

$$\int_0^{\Delta z} e^{-s(z)/\lambda_i}dz = \frac{-\lambda_i}{\left(\frac{ds(z)}{dz}\right)} e^{-s(z)/\lambda_i}\Big|_0^{\Delta z}, \tag{31}$$

giving

$$\Delta\Psi_{m,n_e} = \frac{\Gamma_1^e(\mathbf{\Omega}'\cdot\mathbf{\Omega}'')}{\lambda_e|\mu'||\mu''|}\frac{\lambda_i e^{-(\Lambda_1+\Lambda_2)/\lambda_i}}{\beta-\alpha}[e^{-\alpha\Delta z/\lambda_i} - e^{-\beta\Delta z/\lambda_i}], \tag{32}$$

where Λ_1 and Λ_2 denote the path lengths traveled before the considered segment. The parameters α and β depend on the directions of the trajectory pair along the overlapping segment and are given in Table II. Finally the elastic reflection coefficient is evaluated via

$$\eta_e \equiv C_0 = \frac{|\mu|\Delta\Omega}{N_{\text{pair}}}\sum_{n_e=1}^{\infty}\sum_{m=0}^{n_e-1}\frac{\Psi_{m,n_e}}{n_e}, \tag{33}$$

where the factor $|\mu|$ again effects the trajectory reversal of the outgoing part of each trajectory. The number of trajectory pairs N_{pair} was chosen 10^4 for Au and Cu, and 10^5 for Al and Be.

IV. RESULTS AND DISCUSSION

The angular distributions of electrons of several energies backscattered from Be and Au surfaces calculated with the approaches discussed above are compared in Fig. 3 and Fig. 4 for normal incidence (left panels) and for oblique incidence of 75° with respect to the surface normal (right panels). The latter incidence angle corresponds to an emission angle of −75° in Fig. 3 and Fig. 4.

The oscillations with emission angle seen in the curves for Au are a consequence of the shape of the differential elastic-scattering cross section that exhibits quantum mechanical interferences between the incoming wave and the scattered wave. This phenomenon is similar to the famous Ramsauer–Townsend effect when the elastic cross section for scattering from noble gas atoms even entirely vanishes for a given energy.[39] These oscillations in the cross section, that are sometimes referred to as generalized Ramsauer–Townsend oscillations, are more pronounced for low energies and high atomic numbers.

The results of the conventional MC calculations are represented by open circles, while the data generated with Al-

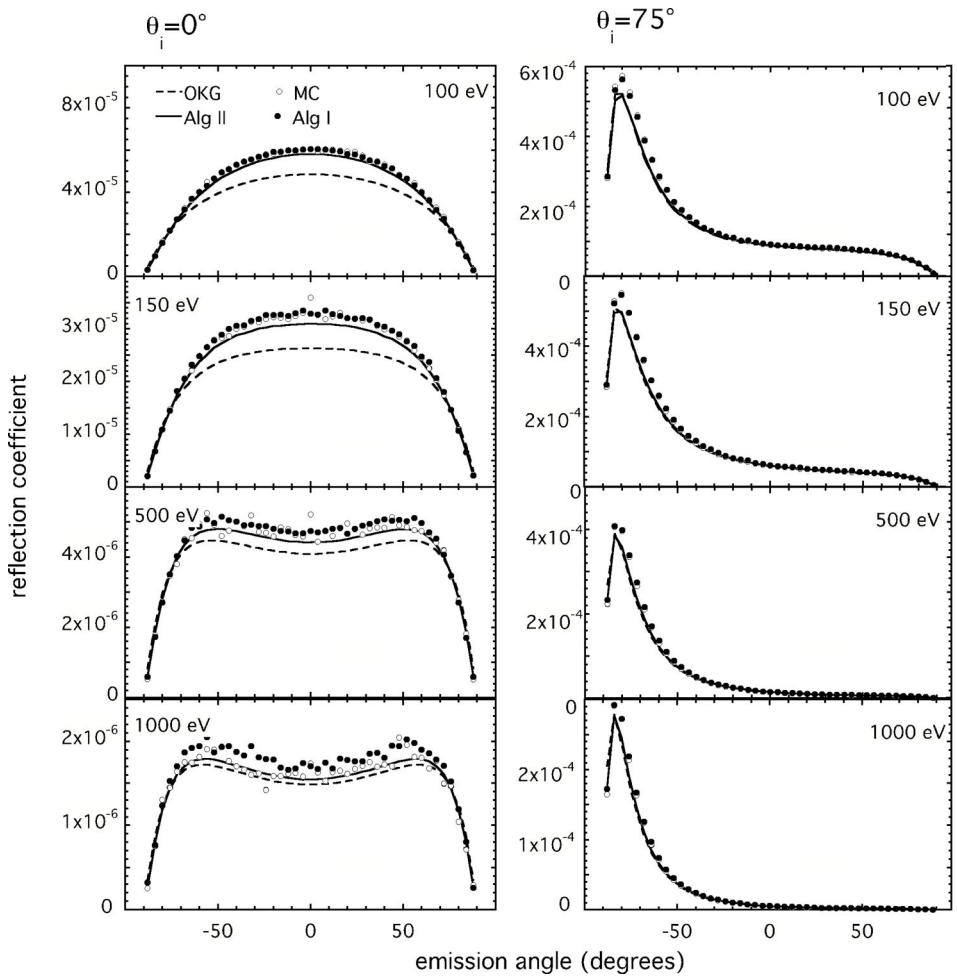

FIG. 3. Differential reflection coefficients for electrons of various energies reflected from a Be surface for normal incidence (left panels) and for an incidence angle of 75° (corresponding to an emission angle of −75°, right panels). Open circles: conventional Monte Carlo calculations (MC). Filled circles: Algorithm I proposed in the present work. Solid lines: Algorithm II proposed in the present work. Dashed lines: Oswald–Kasper–Gaukler Model (OKG).

gorithm I are plotted as filled circles. These two data sets are difficult to distinguish except for cases with significant statistical fluctuations, demonstrating that the two approaches coincide within the statistical uncertainty inherent to MC calculations. This is as expected since the two approaches are essentially equivalent.

The agreement of the OKG model with the MC results is seen to be reasonable in all studied cases, but significant deviations are nonetheless observed for all energies for both materials. For normal incidence and for low energies (100 and 150 eV) where multiple scattering is more significant, the deviations exceed 30%. Note that the importance of multiple scattering is indicated by the value of the scattering parameter χ.[5] For values of χ of the order of unity or higher, a significant multiple scattering contribution is expected, while for ($\chi \ll 1$), multiple scattering becomes less significant (see Table I). For the other energies where the scattering parameter is small $\chi \ll 1$ the deviations are smaller but still of the order of 10% as a rule. For off-normal incidence, the agreement between the OKG model and the MC results is excellent for any energy except for emission angles close to the incident direction where deviations of the order of 10% are again observed.

The results of Algorithm II for normal incidence are seen to agree significantly better with the conventional MC results than the OKG model: for low energies the deviations remain below 10% while for energies above 150 eV the deviations are typically less than 5%. It should be noted that the case of 100 eV electrons normally incident on a Au surface exhibited the largest deviations observed for all materials (including Cu and Al), energies and scattering geometries studied. Since the single scattering term is exact for both the OKG model and Algorithm II, this improvement of the results is attributable to the treatment of multiple scattering. For oblique incidence, Algorithm II and the OKG model are in very close agreement in all cases and compare excellently with the conventional MC results except for scattering geometries corresponding to a deep minimum in the cross section and along the incident direction. This behavior has a clear physical explanation: the elastic cross section always exhibits a strong peak in the forward direction, resembling the Rutherford cross section for a screened Coulomb potential that decreases as $\propto 1/(1-\mu_s)^2$ with the cosine of the scattering angle μ_s. Therefore the cross section for geometries corresponding to small net scattering angles is always rather high

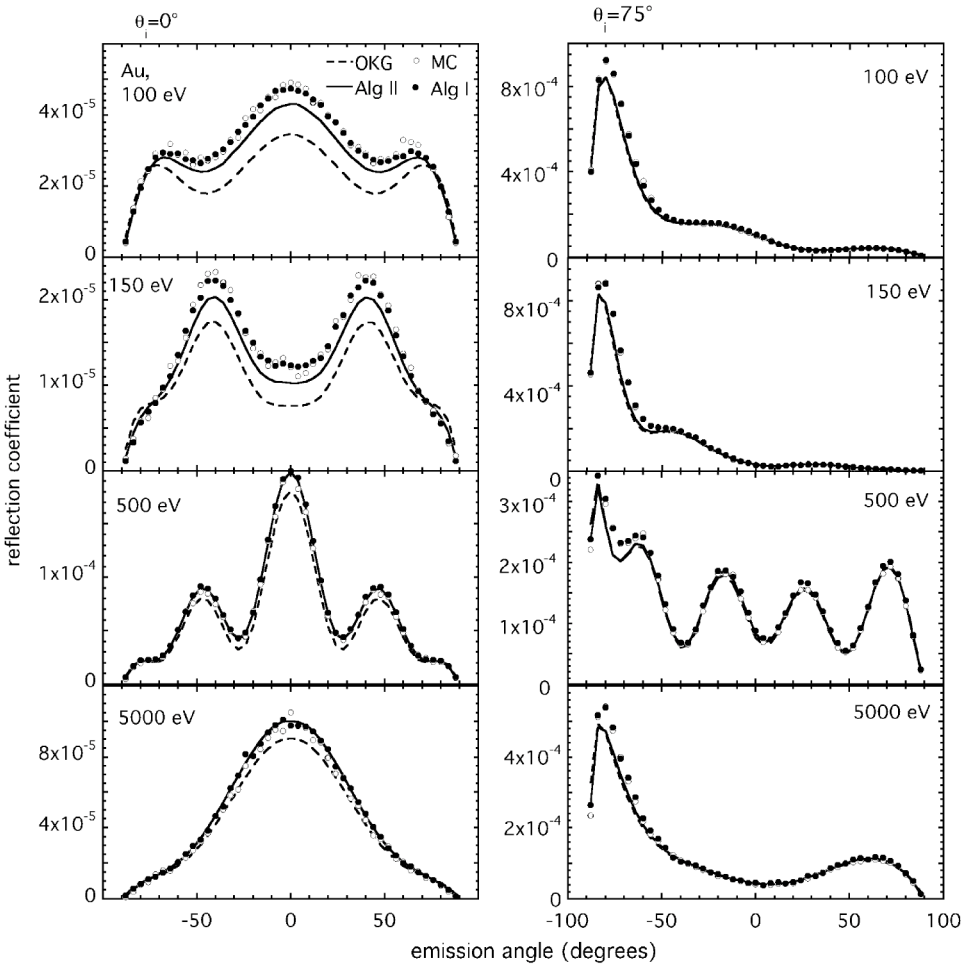

FIG. 4. Same as Fig. 3 for Au.

and the single-scattering term dominates, which is treated exact in both discussed models (see also Fig. 5). For backscattering along directions close to the incident direction, the value of the cross section is much lower so that more elastic events are required for the electron to attain the proper emission direction. In other words, here the multiple scattering term becomes more important which is only treated approximately in both models. This trend can be clearly distinguished in Figs. 3–5, and explains the larger deviations for these geometrical configurations.

In Fig. 5, results of conventional Monte Carlo (MC) calculations for backscattering from a Cu surface are compared with the OKG model (dashed curves) as well as Algorithm II proposed in the present work (solid curves). The data points are the results of conventional Monte Carlo calculations, circles represent the total solution, while diamonds are the contribution of electrons that are deflected only once and the triangles represent the sum of the higher-order scattering contributions. These calculations were performed for an incidence angle of −60° with respect to the surface normal, corresponding to an emission angle of +60°. The single-scattering contribution of the OKG model perfectly matches the MC data, since the OKG model is exact for this case. Note that the single-scattering contribution constitutes by far the largest part of the reflection coefficient (except for scattering angles where the cross section exhibits a deep minimum), which is typical for medium-energy electrons. The higher-order contribution is slightly underestimated by the OKG model. This can be understood by noting that, due to finite deflection angles, the path length for a given depth is always larger than βz used in Eq. (17). Since the probability for multiple scattering increases with the traveled path length, this implies that the OKG model underestimates the multiple scattering probability for any particular depth and consequently also for the total reflection coefficient, as commonly recognized.[4] Nonetheless the agreement of the total reflection coefficient within the OKG model with the MC data is very good: the deviations for the considered case do not exceed 8%.

The multiple-scattering contribution obtained with Algorithm II agrees better with the direct Monte Carlo result while the single-scattering contribution is also exact. In consequence, the total reflection coefficient agrees better with the direct Monte Carlo approach than the OKG result.

The essential difference between the OKG model and Algorithm II, the neglect of the path length elongation due to small-angle scattering, is illustrated in detail in Fig. 6 that shows the quantity $\Psi_{n_e}(z,\mathbf{\Omega})$ for 100 eV electrons normally incident on a Au surface; this is the case for which the largest deviations are observed between the two models. The solid lines are the present approach, calculated with the MC technique, the dashed lines are the result in the OKG model, described by

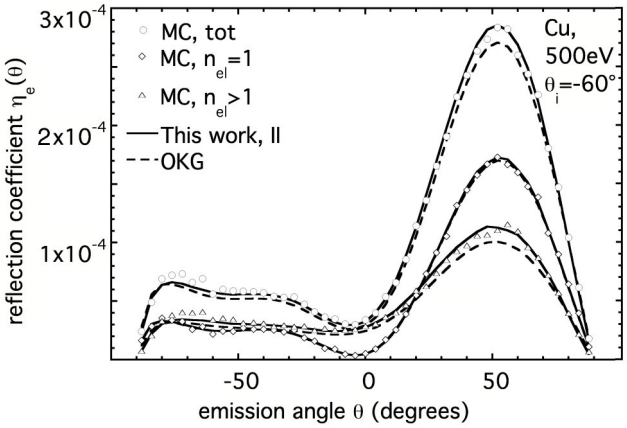

FIG. 5. Differential reflection coefficients for 500 eV electrons reflected from a Cu surface for an incidence angle of −60° (corresponding to an emission angle of +60°). Circles: Monte Carlo calculations for the total reflection coefficient. Diamonds: contribution of electrons which experienced a single elastic collision. Triangles: contribution of higher order elastic scattering. Solid lines: Algorithm II proposed in the present work. Dashed lines: Oswald–Kasper–Gaukler Model (OKG).

$$\Psi_{n_e,n_i=0}(z,\mathbf{\Omega}) = (z/\lambda_e\mu)^{n_e}\frac{e^{-z/\lambda\mu}}{n_e!}. \tag{34}$$

For the straight-line term ($n_e=0$) the two approaches coincide, while for higher orders the path length elongation owing to elastic scattering leads to a significant increase of the contribution of multiple scattering, as given by the area under these curves.

As a final result, Fig. 7 displays the total fraction of medium-energy electrons backscattered into the hemisphere above the sample as a function of the scattering parameter

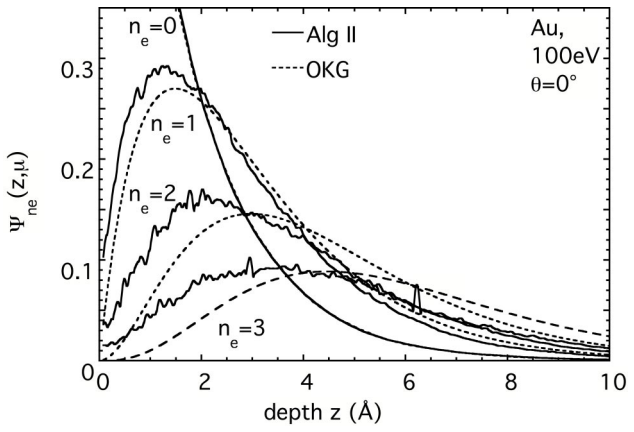

FIG. 6. Escape probabilities $\Psi_{n_e}(z,\mathbf{\Omega})$ [Eq. (27)] for 100 eV electrons normally incident on a Au surface and for normal emission. These quantities are the probability distribution for an electron to escape from the depth z after n_e elastic and no inelastic collisions into the specified direction. The solid curves represent the escape probabilities evaluated with the MC algorithm described in the text, the dashed curves are the result of the OKG model, given by Eq. (34).

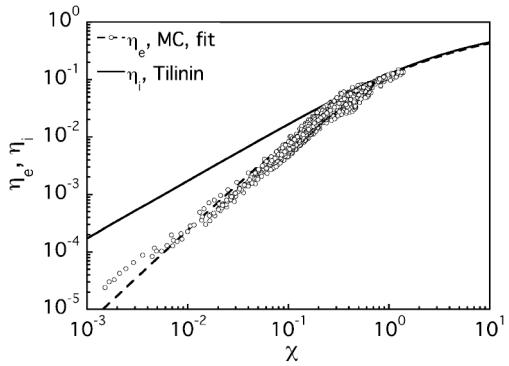

FIG. 7. Total reflection coefficient for a large number of materials and electron energies as a function of the scattering parameter $\chi=\lambda_i/\lambda_{tr}$ (see text). The solid curve represents Tilinin's universal relationship for the total *inelastic* backscattering coefficient, given by expression (35). The dashed curve is the fit of the data to the empirical relationship for the total *elastic* reflection coefficient proposed in the present work [Eq. (36)].

for a large number of elemental solids (Li, Be, B, C, Mg, Al, Si, K, Ca, Sc, Ti, V, Cr, Mn, Fe, Co, Ni, Cu, Zn, Ga, Ge, As, Se, Rb, Y, Zr, Nb, Mo, Ru, Rh, Pd, Ag, Cd, In, Sn, Sb, Te, Cs, Ba, La, Ce, Pr, Nd, Sm, Eu, Gd, Tv, Dy, Ho, Er, Tm, Yb, Lu, Hf, Ta, W, Re, Os, Ir, Pt, Au, Hg, Tl, Pb, Bi). The considered energies were: 50 eV, 100–1000 eV in 100 eV steps and 1000–10000 eV in 1000 eV steps. The calculations were performed for normal electron incidence. Benefiting from the high computational efficiency of Algorithm I, all of these calculations could be performed within 30 min on a PC. The results are shown as open circles in Fig. 7.

For the integral *inelastic* backscattering coefficient, Tilinin[40] found a universal dependence on the scattering parameter σ in the continuous slowing down regime:

$$\eta_i^{\mathrm{tot}} = \frac{\sqrt{1+\sigma}-1}{\sqrt{1+\sigma}+1.9}, \tag{35}$$

where $\sigma=R/\lambda_{tr}$ represents the scattering parameter in the continuous-slowing-down approximation and R is the linear range, i.e., the path length traveled by the particle until its energy is dissipated in the solid. Expression (35) is shown as a function of the quasielastic scattering parameter χ as the solid curve in Fig. 7. For large values of χ (corresponding mainly to low energies) the elastic reflection coefficient, represented by the circles, is seen to closely match this universal curve. Note that for low energies one has $\lambda_i \approx R$ and, furthermore, that the elastic peak makes up a significant fraction of the total backscattered intensity. The elastic-backscattering coefficient also approximately exhibits a universal dependence on the quasielastic scattering parameter: the spread of the reflection coefficient does not exceed a factor of 3 for any value of the scattering parameter while the rms deviation is much less. Therefore, the following empirical formula for the integral backscattering coefficient is proposed that may serve as a guide to estimate this quantity for any material and energy:

$$\eta_e^{\mathrm{tot}} = a_1 \chi^{a_2} \frac{\sqrt{1+\chi}-1}{\sqrt{1+\chi}+2\chi}. \quad (36)$$

The dashed line represents the best fit of the data points to this function. The values of the parameters giving the best fit are: $a_1 = 0.96 \pm 0.02$, $a_2 = 0.65 \pm 0.01$.

V. SUMMARY AND CONCLUSIONS

Backscattering of medium energy electrons has been studied theoretically. Analysis of the kinetic equation for radially symmetric scattering potentials shows that the Green's function for an infinite medium can be expressed in terms of fluctuations in the energy losses and deflection angles on the one hand and the associated collision statistics on the other hand. Although the Green's function was derived for an infinite medium, the form of the solution demonstrates that satisfying the boundary conditions is always possible for an arbitrary problem by finding the appropriate collision statistics since the fluctuation part of the Green's function is independent of the boundary conditions.

For medium-energy electrons, of special interest for the present work, the interaction with the electronic and ionic subsystem can be decoupled and the loss function is further simplified. On this basis it was possible to find the exact solution of the elastic backscattering problem, Eq. (22), that was introduced as Algorithm I. An effective approximation is obtained by introducing the approximate angular correlations [Eq. (23)]. The ensuing procedure to calculate the backscattering coefficient [Eq. (24)] is introduced as Algorithm II. An additional approximation can be made in which the path length elongation due to small-angle scattering is neglected [Eq. (18)]. Combining the two approximations addressed above leads to the Oswald–Kasper–Gaukler (OKG) model[26] [Eq. (19)].

While the OKG model can be integrated analytically leading to a closed expression for the partial elastic-reflection coefficient [Eq. (20)], Algorithm I and II can be implemented in an efficient MC procedure based on the trajectory-reversal technique. The computational speed is independent of the detector acceptance angle, which constitutes a significant advantage over conventional MC algorithms where the effort of calculation increases drastically for small detector solid angles. Comparison with results of conventional MC calculations demonstrates that Algorithm I is exactly equivalent to the conventional MC procedure, while the computational efficiency of the latter is several orders of magnitude higher. The approximate algorithm turns out to be quite accurate, always leading to a significant improvement over the OKG model. Deviations with conventional MC calculations are typically less than 5% for energies exceeding 200 eV. Since the experimental error in EPES is of the same order of magnitude, both presented algorithms may be used for determination of the IMFP by means of EPES. Although this was not explicitly demonstrated, both algorithms are applicable to arbitrary surface morphologies and can cope in a simple way with depth-dependent interaction characteristics such as surface excitations.

The integral backscattering coefficient for normal incidence was found to follow a universal relationship with the scattering parameter to a good approximation, making it possible to estimate this quantity for an arbitrary energy and material in a simple way.

ACKNOWLEDGMENTS

Financial support of the present work by the Austrian Science Foundation FWF through Project No. P15938-N02 is gratefully acknowledged.

*Electronic address: werner@iap.tuwien.ac.at; Fax: +43-1-58801-13499; Tel: +43-1-58801-13462

[1] R. Schmid, Ph.D. thesis, University of Tübingen, Germany, 1982.
[2] R. Oswald, Ph.D. thesis, Eberhard-Karls-Universität Tübingen 1992.
[3] C. J. Powell and A. Jabłonski, J. Phys. Chem. Ref. Data **28**, 19 (1999).
[4] A. Dubus, A. Jabłonski, and S. Tougaard, Prog. Surf. Sci. **63**, 135 (2000).
[5] W. S. M. Werner, Surf. Interface Anal. **31**, 141 (2001).
[6] W. S. M. Werner, in *Surface Analysis by Auger and X-Ray Photoelectron Spectroscopy*, edited by D. Briggs and J. Grant (IMPublications, Chichester, UK, 2003).
[7] J. S. Schilling and M. B. Webb, Phys. Rev. B **2**, 1665 (1970).
[8] G. Gergely, Prog. Surf. Sci. **71**, 31 (2002).
[9] A. Jabłonski, Surf. Interface Anal. **29**, 582 (2000).
[10] W. S. M. Werner, C. Tomastik, T. Cabela, G. Richter, and H. Störi, Surf. Sci. **470**, L123 (2001).
[11] W. S. M. Werner, C. Tomastik, T. Cabela, G. Richter, and H. Störi, J. Electron Spectrosc. Relat. Phenom. **113**, 127 (2001).
[12] C. J. Powell, Surf. Sci. **44**, 29 (1974).
[13] C. J. Powell, J. Electron Spectrosc. Relat. Phenom. **47**, 197 (1988).
[14] C. J. Powell and M. P. Seah, J. Vac. Sci. Technol. A **8**, 735 (1990).
[15] W. Smekal, W. S. M. Werner, C. S. Fadley, and M. A. van Hove, J. Electron Spectrosc. Relat. Phenom. **137**, 183 (2004).
[16] K. M. Case and P. F. Zweifel, *Linear Transport Theory* (Addison–Wesley, Reading, MA, 1967).
[17] W. H. Gries and W. S. M. Werner, Surf. Interface Anal. **16**, 149 (1990).
[18] I. S. Tilinin and W. S. M. Werner, Phys. Rev. B **46**, 13 739 (1992).
[19] W. S. M. Werner, I. S. Tilinin, and A. Jabłonski, Surf. Interface Anal. **23**, 823 (1995).
[20] S. Chandrasekhar, *Radiative Transfer* (Dover, New York, 1960).
[21] B. Davison, *Neutron Transport Theory* (Oxford University Press, Oxford, 1955).
[22] A. Jabłonski, C. Jansson, and S. Tougaard, Phys. Rev. B **47**, 7420 (1993).

[23] B. Tombuyses and A. Dubus, Math. Comput. Simul. **47**, 483 (1998).
[24] W. S. M. Werner, I. S. Tilinin, and M. Hayek, Phys. Rev. B **50**, 4819 (1994).
[25] Y. F. Chen, P. Su, C. M. Kwei, and C. J. Tung, Phys. Rev. B **50**, 17 547 (1994).
[26] R. Oswald, E. Kasper, and K. Gaukler, J. Electron Spectrosc. Relat. Phenom. **61**, 251 (1993).
[27] V. M. Dwyer, Surf. Interface Anal. **20**, 513 (1993).
[28] A. Jabłonski, B. Lesiak, and G. Gergely, Phys. Scr. **39**, 363 (1989).
[29] M. Vicanek, Surf. Sci. **440**, 1 (1999).
[30] L. Glazov and S. Tougaard, Phys. Rev. B **68**, 155409 (2003).
[31] R. H. Ritchie, Phys. Rev. **106**, 874 (1957).
[32] R. Nunez, P. M. Echenique, and R. H. Ritchie, J. Phys. C **13**, 4229 (1980).
[33] W. S. M. Werner, Surf. Sci. **526/3**, L159 (2003).
[34] L. D. Landau, J. Phys. (Moscow) **8**, 201 (1944).
[35] W. S. M. Werner and P. Schattschneider, J. Electron Spectrosc. Relat. Phenom. **142**, 65 (2005).
[36] S. Goudsmit and J. L. Saunderson, Phys. Rev. **57**, 24 (1940).
[37] S. Tanuma, C. J. Powell, and D. R. Penn, Surf. Interface Anal. **21**, 165 (1994).
[38] F. Salvat and R. Mayol, Comput. Phys. Commun. **74**, 358 (1993).
[39] P. Schattschneider, *Fundamentals of Inelastic Electron Scattering* (Springer, New York, 1986).
[40] I. S. Tilinin, Sov. Phys. JETP **55**, 751 (1982).